ACS OMEGA

http://pubs.acs.org/journal/acsodf
Article

Cobalt Ferrite Surface-Modified Carbon Nanotube Fibers as an Efficient and Flexible Electrode for Overall Electrochemical Water Splitting Reactions

Aneesa Fatima, Haia Aldosari, M. S. Al-Buriahi, Maryam Al Huwayz, Z. A. Alrowaili, Mohammed S. Alqahtani, Muhammad Ajmal, Arif Nazir, Munawar Iqbal,* Raqiqa Tur Rasool,* Sheza Muqaddas,* and Abid Ali*

Cite This: *ACS Omega* 2023, 8, 37927−37935

ABSTRACT: One of the most practical and environmentally friendly ways to deal with the energy crises and global warming is to produce hydrogen as clean fuel by splitting water. The central obstacle for electrochemical water splitting is the use of expensive metal-based catalysts. For electrocatalytic hydrogen production, it is essential to fabricate an efficient catalyst for the counterpart oxygen evolution reaction (OER), which is a four-electron-transfer sluggish process. Here in this study, we have successfully fabricated cobalt-based ferrite nanoparticles over the surface of carbon nanotube fiber (CNTF) that was utilized as flexible anode materials for the OER and overall electrochemical water splitting reactions. Scanning electron microscopy images with elemental mapping showed the growth of nanoparticles over CNTF, while electrochemical characterization exhibited excellent electrocatalytic performance. Linear sweep voltammetry revealed the reduced overpotential value (260 mV@$\eta_{10mAcm-2}$) with a small Tafel slope of 149 mV dec^{-1}. Boosted electrochemical double layer capacitance (0.87 mF cm^{-2}) for the modified electrode also reflects the higher surface area as compared to pristine CNTF (C_{dl} = 0.022 mF cm^{-2}). Charge transfer resistance for the surface-modified CNTF showed the lower diameter in the Nyquist plot and was consequently associated with the better Faradaic process at the electrode/electrolyte interface. Overall, the as-fabricated electrode could be a promising alternative for the efficient electrochemical water splitting reaction as compared to expensive metal-based electrocatalysts.

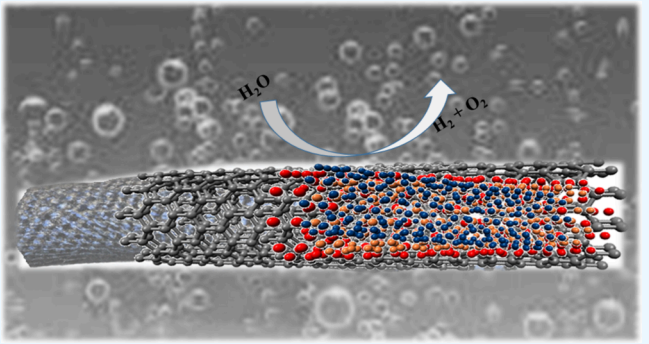

1. INTRODUCTION

No doubt nonrenewable sources of energy are the backbone of the global economy for many decades, but they have several damaging environmental impacts including hazardous greenhouse gas emission, air pollution, and diverse climate changes.[1,2] Nearly 79% of economy has been relying on the fossil fuels, which are nonrenewable energy sources such as coal, oil, and natural gases.[3−5] The cumulative rate of fossil fuel burning boosts up the emission of greenhouse gases (CO_2 and NO_2), which also cause the reduction of nonrenewable energy resources along with harmful environmental impact.[6] These issues encouraged the research community to develop plentiful, durable, zero emission and environmentally friendly technology as an alternative energy.[7,8]

To this end, hydrogen, as a clean and carbon-free renewable energy source, is a tremendous fuel with limitless potential and recycling advantage. Compared to gasoline, which has 44 MJ/kg energy density, hydrogen is the lightest with the highest energy density of 120 MJ/kg[9] with only water as a byproduct during combustion.[10,11] In addition to being a possible long-term fuel, hydrogen is also employed in a variety of industrial processes, including the generation of methanol and ammonia and crude oil hydrocracking.[12,13] Diverse approaches, including nuclear power, natural gas, coal, biomass, and water splitting, could be used to generate hydrogen gas.[14−16] Among all, water splitting via thermal, electrochemical, and photoelectrochemical processes has intensive advantages over all procedures. Electrochemical water splitting has the following mechanism with anodic and cathodic processes for OER and HER, respectively.[17,18]

Anodic process:

Received: May 12, 2023
Accepted: August 30, 2023
Published: October 4, 2023

https://doi.org/10.1021/acsomega.3c03314
ACS Omega 2023, 8, 37927−37935

$$OH^- \rightarrow \frac{1}{2}O_2 + \frac{1}{2}H_2O + 2e^-(E_o = +0.40 \text{ vs RHE}) \quad (1)$$

Cathodic process:

$$H_2O + 2e^- \rightarrow 2OH^- + H_2(E_o = -0.83 \text{ vs RHE}) \quad (2)$$

Overall process:

$$H_2O \rightarrow \frac{1}{2}O_2 + H_2(E_o = -1.23 \text{ vs RHE}) \quad (3)$$

The anodic process (eq 1) is related to oxygen evolution reaction in which hydroxyl ions release their electrons at the anode during water electrolysis and are oxidized to liberate the oxygen gas, while reduction occurs at the cathode with the liberation of hydrogen as elaborated in eq 2.

High-quality hydrogen is generated when water molecules are split into their constituent elements of H_2 and O_2 using electrocatalysts; in reality, a considerable amount of energy is required for the reaction.[19−21] The thermodynamic potential (E_o) required for electrochemical splitting of water is 1.292 V (vs RHE) with 237.1 kJ mol^{-1} Gibbs free energy, which must be provided to the electrolyzer to initiate the process. Equation 4 represents the following process:

$$2H_2O \rightarrow 2H_2 + O_2 \quad \Delta G = 237.21 \text{ kJ mol}^{-1} \quad (4)$$

where ΔG is the Gibbs free energy associated with energy absorbed during the water dissociation reaction. Hydrogen produced by water splitting has zero impact on the environment because water is used as raw material and can be continuously recycled back into nature, making it a closed-loop process that does not produce fossil fuel-related pollution.[22] To promote the process having economic worth, oxygen, a byproduct with no negative environmental effects, can be utilized in different ways. The process of electrolysis, which involves breaking the hydrogen bonds within water molecules, demands a significant amount of energy. This high energy requirement, coupled with the substantial expenditure involved, limits the widespread use of water electrolysis for hydrogen production. As a result, electrolysis currently represents ∼4% of the overall global hydrogen production.[23−25] Water dissociation into H_2 and O_2 involves two crucial reactions, which includes hydrogen evolution as a cathodic process and oxygen evolution as an anodic process given in eqs 1 and 2, respectively. However, OER reaction exhibits inherently slow kinetics and consequently proceeds at a relatively sluggish rate.[26,27] This sluggishness in electrode kinetics implies a challenge for efficient and rapid water dissociation processes.[28−30] To make a process smooth, a catalyst must be used to help break down the strong chemical bonds in the water molecule.

Currently, metal-based materials (Pt, RuO, and IrO) and their derivatives have demonstrated good performance in electrochemical[31,32] and photocatalytic water splitting.[33,34] These metal-based electrocatalysts hindered the practical implementation of hydrogen production via water splitting due to abundance in nature, high cost, and corrosion issues.[35,36] Therefore, the pursuit of transition metals and their compounds as catalysts holds great promise for achieving efficient and scalable catalytic processes, marking a significant advancement in the field of catalysis.[33,36−40]

Due to their varied nanostructures, transition metal oxides have received a lot of attention as cutting-edge electrocatalysts including their oxides,[41] oxyhydroxides,[42] and phosphates.[43−45] Metal−organic frameworks (MOFs) also played a significant role in electrochemical water splitting to get the clean hydrogen fuels efficiently.[46−48] Medium entropy alloys of multimetals showed the enhanced electrocatalytic performance for methanol oxidation along with OER and HER.[49] Ferrite materials such as MFe_2O_4 (M = Co,[50−52] Ni,[53−56] Cu, Fe,[57−59] etc.) have shown potential for applicability to OER electrocatalysis with promising characteristics. The electrocatalytic activity of ferrite structures is significantly influenced by the electronic transitions occurring between different metal valences in the oxygen (O) sites. These electronic transitions play a vital role in determining the catalytic behavior and efficiency of ferrite material. Apart from their advantageous electronic properties, ferrite structures possess a significant attribute of a surface redox active metal center. The central part of these metals assists as key spots, which help for the better adsorption and activate the electroactive species in an efficient way. By offering these active sites on their surface, ferrite structures enable the efficient binding and subsequent transformation of electroactive species, thereby enhancing their overall catalytic activity.[60−62]

$CoFe_2O_4$ stands out as an exceptionally captivating ferrite due to its compelling combination of advantageous attributes. Notably, its low cost, abundance, and lower toxicity render it highly desirable for numerous applications. Unfortunately, higher volume expansion and lower conductivity for the pure ferrites ($CoFe_2O_4$) restrict the utilization of these types of materials in pristine form. As a result, extensive efforts have been made to enhance the electrocatalytic properties for practical implementation. A porous $CoFe_2O_4$/C nanorod array with good OER performance was reported by Lu et al.[63] $CoFe_2O_4$ nanospheres were created by Yan et al., demonstrated good OER activity with a hollow structure and greater surface area, and exhibited more vacancies than other materials.[64−66] Rana et al. conducted a study on the effects of Co_2FeO_4 nanostructures, synthesized via a hydrothermal route.[67] Their findings indicated that nanoparticles of cobalt ferrite exhibited an overpotential value of 560 mV with a Tafel slope of 160 mV dec^{-1} for OER. Zhang et al. investigated the performance of Co_2FeO_4 toward OER at different temperatures and found that at high temperature, Co_2FeO_4 displayed a reduced Tafel slope value of 159 mV dec^{-1} with an overpotential value of 446 mV at 10 mA cm^{-2} current density.[68]

Here, in this work, we prepared cobalt-based ferrite ($CoFe_2O_4$) nanoparticles with a diameter of ∼70 nm using a hydrothermal process and deposited them over the surface of CNT fiber. $CoFe_2O_4$@CNTs composite fiber exhibited a splendid performance toward electrochemical water splitting in basic media with larger active surface area and multiple active sites. The one-dimensional shape of the composite electrode facilitates electron transport and reduces the path length for charge transfer, leading to improved electrical conductivity and enhanced electrocatalytic activity. Hence, $CoFe_2O_4$ nanoparticles show better conductivity, improved stability, and hence, excellent electrocatalytic performance for overall electrochemical water splitting reactions in alkaline media. Additionally, at an applied potential of 1.57 V (η = 340 mV), chronoamperometric performance demonstrated excellent stability for both anodic and cathodic processes (overall electrochemical water splitting).

https://doi.org/10.1021/acsomega.3c03314
ACS Omega 2023, 8, 37927−37935

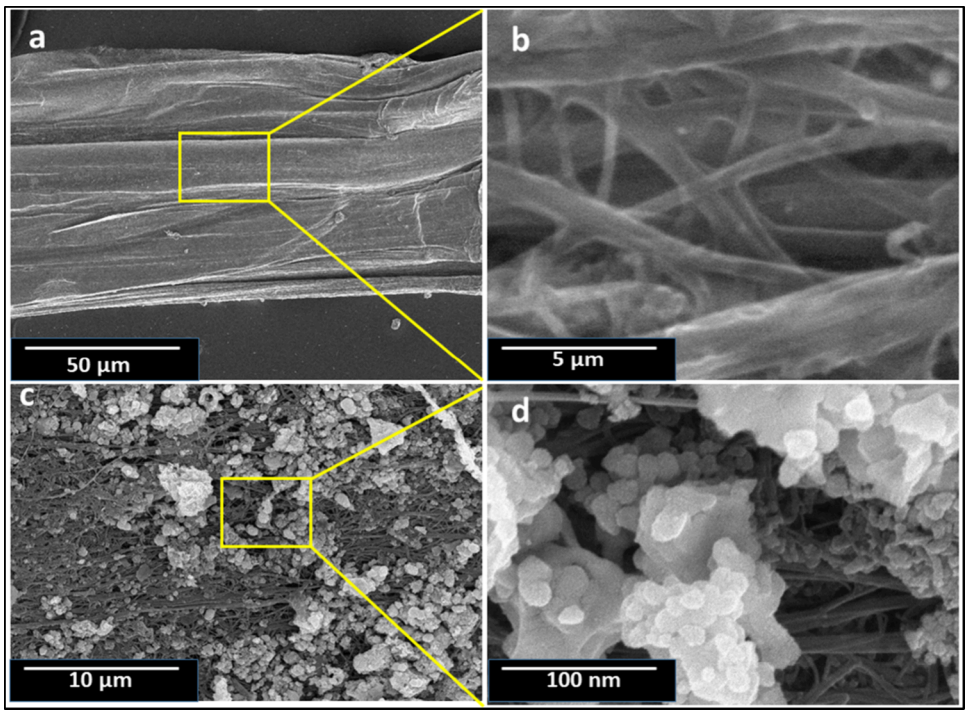

Figure 1. SEM images for (a, b) bare and (c, d) $CoFe_2O_4$ nanoparticle-modified CNTFs at lower and higher magnifications.

2. EXPERIMENTAL SECTION

2.1. Chemicals. All used chemicals were purchased from Sigma-Aldrich, and ferrous sulfate heptahydrate ($FeSO_4 \cdot 7H_2O$), urea (CH_4N_2O), cobalt chloride hexahydrate ($CoCl_2 \cdot 6H_2O$), potassium hydroxide (KOH), and Nafion (5 wt %) were used with analytical grade purity. All solvents were also of analytical grade throughout the experiments and were used without further purification, while deionized water was utilized exclusively throughout the experimental procedures.

2.2. Fabrication of $CoFe_2O_4$-Modified CNTF. Forty milliliters of deionized water was used to dissolve 2 mM iron(II) sulfate ($FeSO_4 \cdot 7H_2O$) and 1 mM cobalt(II) chloride ($CoCl_2 \cdot 6H_2O$) solution. Under vigorous stirring, 10 mM urea was added to the above mixture and stirred for further 20 min. After complete dissolution, the resulting solution was transferred into a 25 mL stainless steel autoclave with a Teflon lining inside. A glass substrate, on which (CNTF) was previously attached, was placed inside the autoclave. The autoclave was tightly closed and put inside an electric oven at a fixed temperature of 160 °C for 8 h, which allows this reaction to grow the nanomaterials over the CNTF surface. After completion, the reaction was let to cool down at room temperature and CNTF was washed with ethanol and water thoroughly in a sequential manner to eliminate any residues and contaminants. The nanoparticle-modified electrode ($CoFe_2O_4$@CNTF) attached onto another substrate with an indium connection as an electrode to study electrochemical performance. To check the catalytic activity for the pure $CoFeO_4$, the slurry for the as-synthesized material was formulated in the Nafion solution (10%) and drop-casted over the surface of the glassy carbon electrode, which was used as a working electrode during analysis.

2.3. Characterization. Scanning electron microscopy was carried out via a Hitachi SEM S-4800 (1 kV) machine to analyze the surface morphology of pristine and modified CNT fiber. A Bruker D8 Advance XRD instrument was employed for the crystalline behavior measurements. Electrochemical measurements were taken via a Gamry Reference 3000 Potentiostat/Galvanostat. A Biosafer deionizer was employed to get deionized water, which was used throughout the experiments.

2.4. Electrochemical Measurements. Electrochemical-related studies were investigated using a three-electrode setup with modified CNTF, Pt, and Ag/AgCl as working, counter, and reference electrodes, respectively. Polarization curves were obtained via linear sweep voltammetric (LSV) studies for the OER in alkaline media (1 M KOH) at a fixed scan rate of 5 mV/s. *i-R* compensation (CI) was used while taking the voltammograms. Electrochemical double layer capacitance was calculated via cyclic voltammetry, taken at various scan rates with the fix concentration of electrolyte in the nonfaradaic potential region. The interfacial charge transfer phenomenon was estimated using AC impedance spectroscopy with the current frequency range from 0.1 Hz to 1 MHz at DC potential in the faradaic region (0.6 V) and a small sinusoidal potential (5 mV). All the measured potentials were converted with respect to RHE (reversible hydrogen electrode) using the formulation given in eq 5.

$$E_{RHE} = E_{Ag/AgCl} + 0.059pH + E_{oAg/AgCl} \quad (5)$$

where $E_{oAg/AgCl}$ is the electrode potential (0.1976 V) under the standard condition for silver/silver chloride at 25 °C, $E_{Ag/AgCl}$ is the measured potential away from equilibrium, and E_{RHE} is the converted potential against the reversible hydrogen electrode.

3. RESULTS AND DISCUSSION

SEM was utilized to investigate the surface morphology of bare and $CoFe_2O_4$-modified CNT fibers. Figure 1a,b displays the densely populated pristine CNT fibers, which offer higher mechanical strength and numerous pathways for facilitating the movement of electric charges. Compared to CNTs in powdered form, the well-aligned structure of the CNT fiber significantly improves the flow and unhindered movement of

https://doi.org/10.1021/acsomega.3c03314
ACS Omega 2023, 8, 37927−37935

charges, resulting in the improved conductivity. The presence of numerous interfaces in the powdered form of CNTs creates obstacles that hinder the process of electrochemical charge transfer, leading to reduced efficiency in conductivity, while the unidimensional CNTF with its constrained pathway acts as a conductive medium that promotes a smooth and unrestricted flow of charges. This unique characteristic of the CNTF significantly enhances the conductivity and, consequently, boosts the overall performance of the electrodes, surpassing the limitations imposed by the powdered form of CNTs. SEM images presented in Figure 1c,d provide clear visual evidence of the surface-modified CNT fibers at different magnifications. The deposition process demonstrated its effectiveness by achieving successful loading of $CoFe_2O_4$ nanoparticles onto the surface of CNT fibers. This deposition process ensured that nanoparticles were securely attached and uniformly distributed across the entire surface of the CNT fibers, validating the quality and reliability of the modification. The size analysis of the $CoFe_2O_4$ nanoparticles indicated a uniform range of 70−100 nm, ensuring a consistent size distribution within this specific size range. Deposited $CoFe_2O_4$ nanoparticles played a crucial role as electrocatalytic sites specifically involved in hydroxyl ion (OH^-) oxidation during the electrochemical process of water splitting. Simultaneously, the CNT fiber acted as a conduit, providing a clear and defined pathway for the internal flow of electric charges within the system. This collaborative functionality of the deposited nanoparticles and the CNT fiber synergistically enhanced the electrochemical activity of electrode materials by facilitating efficient charge transfer and promoting the desired electrochemical reactions.

Along with SEM, to verify the elemental composition, namely, carbon, cobalt, iron, and oxygen, energy-dispersive X-ray spectroscopy (EDS) analysis was conducted. This technique allows elemental mapping of the sample, providing visual evidence of the homogeneous presence of all the elements across the material. Figure 2 shows the repetitive

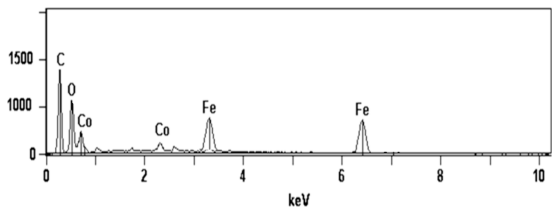

Figure 2. EDX pattern of $CoFe_2O_4$-modified CNT fiber with carbon, iron, cobalt, and oxygen abundant ratio.

abundance and elemental map for carbon, cobalt, iron, and oxygen presented by the highest peak for carbon and relatively lower abundance of cobalt with uniform distribution of each element.

Figure 3 presents the elemental X-ray mapping for $CoFe_2O_4$@CNTF, illustrating the even distribution of C, O, Fe, and Co elements across the surface of the CNTF with different densities. A carbon substrate appears as the area with the highest density, represented by a white color. On the other hand, the Co, Fe, and O elements are associated with distinct colors: violet for Co, green for Fe, and light blue for O. These color variations indicate different elemental compositions and distributions within the $CoFe_2O_4$@CNTF structure.

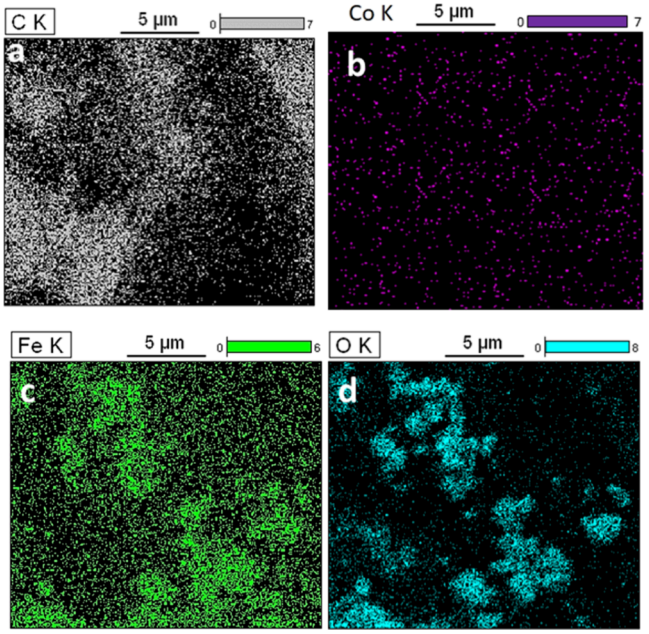

Figure 3. EDX spectra for the elemental X-ray mapping of (a) carbon, (b) cobalt, (c) iron, and (d) oxygen over the surface of $CoFe_2O_4$@CNTF.

The XRD patterns for the pristine carbon nanotubes and their modification with $CoFe_2O_4$ nanoparticles are given in Figure 4. The crystallinity and phase structure of the synthesized $CoFe_2O_4$ nanoparticles are shown by the diffraction pattern. Pristine carbon nanotubes exhibited two peaks corresponding to different planes (002) and (100). A sharp and more intense peak appeared at around 27° of 2θ and a broader peak positioned at 42° equivalent to the (002) and (100) planar values, respectively. The obtained 2θ values of $CoFe_2O_4$ nanoparticle-modified carbon nanotubes are consistent with those of the standard cubic phase $CoFe_2O_4$ and their corresponding (h, k, l) planar values. The planar values of (002), (311), (220), (200), (400), (511), (422), and (440) match with the standard JSPD card for $CoFe_2O_4$. Due to the smaller atomic radius (200 pm), the cobalt materials were produced as spinel ferrites with tetrahedral sites occupied by the iron-coupled cobalt elements.

A conventional three-electrode setup has been used to study the OER performance of bare CNTF, $CoFe_2O_4$ nanoparticles, and modified $CoFe_2O_4$@CNTF in alkaline solution (1 M KOH) as the electrolyte. Figure 5 represents the electrochemical studies for overpotential, double layer capacitance, and charge transfer behavior. LSV in Figure 5a represented the i-R-corrected polarization curves for bare $CoFe_2O_4$ nanoparticles and modified CNTF electrode with a fixed scan rate of 5 mV s^{-1} and a voltage range of 1−2 V vs RHE. The black color voltammogram associated with the surface-modified electrode showed the low overpotential (260 mV) as compared to the pristine CNTF (shown in red) at a current density of 10 mA cm^{-2}. Meanwhile, the blue color represented the pure cobalt-based ferrite nanoparticle, which showed the catalytic performance but less than the fiber-based electrode. This is because the CNTF provided more active sites to nanoparticles and fiber itself as the path flow for the charge transportation. The observed decrease in overpotential of the modified electrode, when compared to the bare CNT fiber, provides compelling evidence of its superior electrocatalytic

https://doi.org/10.1021/acsomega.3c03314
ACS Omega 2023, 8, 37927−37935

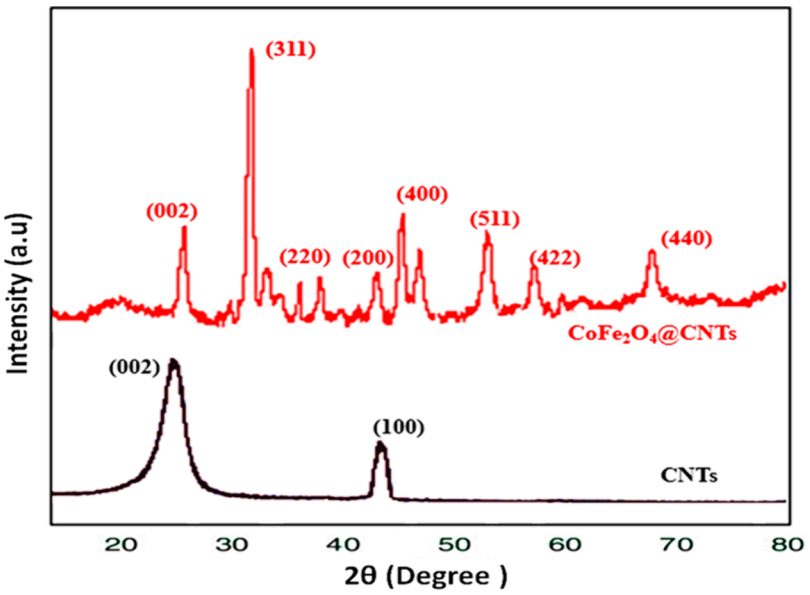

Figure 4. X-ray diffraction pattern for the pristine and modified CNTFs ($CoFe_2O_4$@CNTFs) with the corresponding planes.

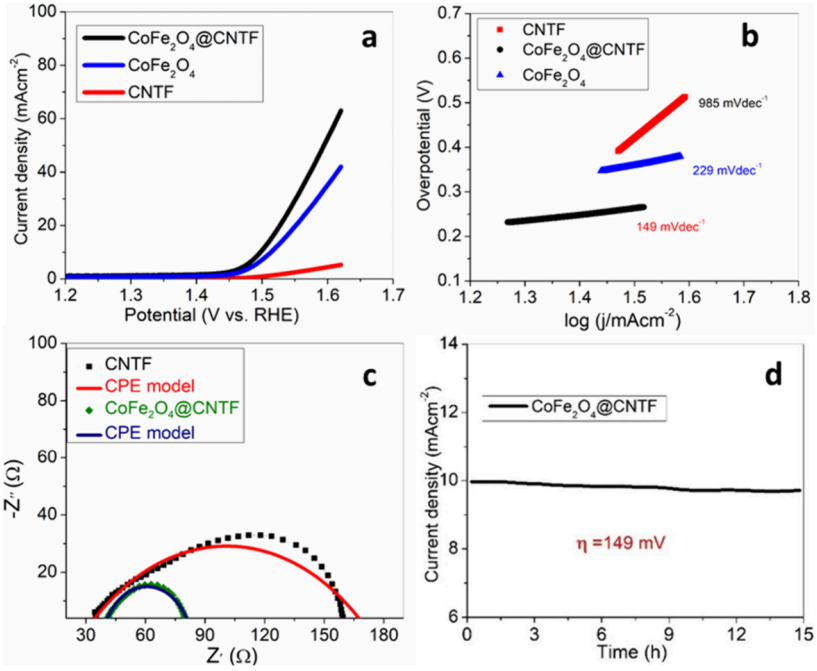

Figure 5. (a) *iR*-compensated polarization curves for OER for the bare CNT fiber and $CoFe_2O_4$ nanoparticle-modified CNTF electrode in 1 M KOH solution at a scan rate of 5 mV s^{-1} and (b) their corresponding Tafel plots. (c) Nyquist plots in electrochemical impedance spectroscopy for bare CNT fiber and modified CNTF with fitted curves and (d) chronoamperometric studies for the modified CNTF at an overpotential of 149 mV.

OER performance. Electrode kinetics for the OER were further explored from the analysis of Tafel slopes (Figure 5b), generated from the polarization curves. Tafel slopes were calculated to be 149, 229, and 985 mV dec^{-1} for modified fiber, cobalt-based ferrite, and bare CNTF, respectively. The lower Tafel slope represented the faster electrode kinetics with a high rate of oxygen evolution reactions at a small amount of voltage. Meanwhile, for pristine CNTF, a higher value of Tafel slope (985 mV dec^{-1}) showed the large amount of energy required in the form of potential to convert the hydroxyl ions into oxygen and, consequently, a slower process. The fiber-based composite electrode also showed its splendid performance as compared to the pure form of $CoFe_2O_4$ nanoparticles at the glassy carbon electrode, which showed a higher Tafel slope (229 mV dec^{-1}), which is due to the less surface area and minor active sites.

Figure 5c represents the Nyquist plots of electrochemical impedance spectroscopy, which predict the charge transfer resistance (R_{ct}) values that elaborate the mechanistic explanations for the OER activity of electrode material. In a Nyquist plot, the diameter of the semicircle observed in the high-frequency region provides information about the charge-transfer resistance at the electrode/electrolyte interface. A larger semicircle diameter indicates a higher resistance, signifying a less efficient electron-transfer process, while a small semicircle on $CoFe_2O_4$@CNTF indicated lower charge-

https://doi.org/10.1021/acsomega.3c03314
ACS Omega 2023, 8, 37927−37935

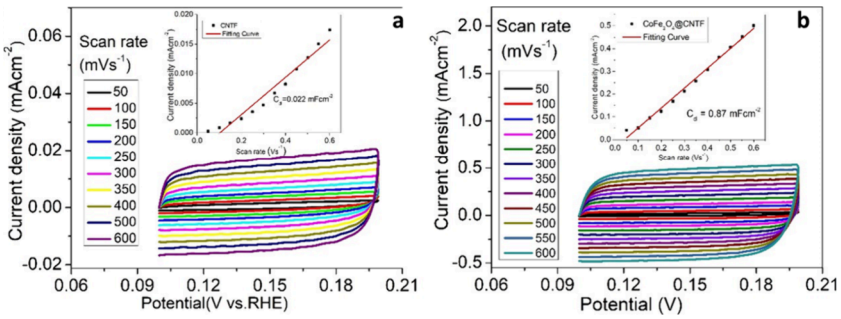

Figure 6. Cyclic voltammogram for (a) pristine and (b) modified CNTF in 1 M KOH solution with varied scan rate in the nonfaradaic region. Inset images represent the linear connection among the current and scan rates to calculate the double layer capacitance.

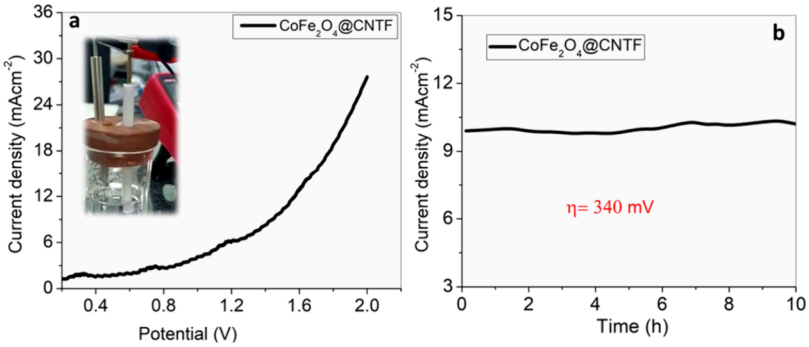

Figure 7. (a) Polarization curve with an optical image (inset) and (b) chronoamperometry for the overall electrochemical water splitting via $CoFe_2O_4$ nanoparticle-modified fibers in 1 M KOH.

transfer resistance (47 Ω) and attained an efficient electron-transfer process for the OER. When compared to pristine layers of CNTF, it showed a semicircle with larger diameter and a R_{ct} value of 145 Ω, which is nearly three times higher as related to the modified electrode, hence the lower electrocatalytic performance toward the OER. Their curve fitting model showed that the solution resistance was almost the same for both modified and pristine electrodes. The stability of the fabricated electrodes with time has been assessed using the chrono method (i–t), specifically by the continuous process of OER in alkaline solution (KOH) with a molarity of 1 M. The experiment was carried out at a constant potential of faradaic region relevant to the current density of 10 mA cm^{-2} for a duration of 15 h. Outcomes of this stability test are depicted in Figure 5d, providing a representation of the electrode's performance over the testing period. The modified CNTF exhibited remarkable stability over an extended period of time, showcasing its promising performance and potential for practical applications. Even after 15 h of electrochemical reaction, the electrode still exhibited activity and the post-SEM analysis showed almost the same surface morphology with little blockage of active sites as shown in Figure S1 in the Supporting Information.

To obtain the electrochemical capacitance (C_{dl}) on the electrode surface, cyclic voltammetry was carried out in the nonfaradaic portion at various scan rate values for both pristine and modified CNTFs. Within the nonfaradaic (charging) region, the capacitive current has been increased with higher scan rate. The current values increased from 0.001 to 0.0017 mA cm^{-2} for pristine CNTF, and it varied from 0.05 to 0.5 mA cm^{-2} for the modified CNTF as displayed in Figure 6a,b, respectively. As shown by the insets in Figure 6, there is a linear relation between the scan rate and the current density. The fitting allowed for the determination of the C_{dl} values, which were calculated to be 0.022 and 0.85 mF cm^{-2} for pristine and modified CNTFs, respectively.

C_{dl} at the electrode–electrolyte interface is an important factor in determining the electrochemical surface area (ECSA) of the electrode material. The greater the double layer capacitance value, the higher will be the ECSA and consequently better the electrocatalytic performance.

3.1. Overall Electrochemical Water Splitting. In addition to their excellent performance as an anode catalyst for OER, cobalt ferrite ($CoFe_2O_4$)-modified fibers have been specifically investigated for their effectiveness as a cathodic material also for hydrogen evolution reaction in complete (overall) water electrolysis. For this, platinum (Pt), as the counter electrode, has been replaced with the same materials ($CoFe_2O_4$@CNTF), which facilitated the HER during water electrolysis. Studies of cobalt ferrite ($CoFe_2O_4$) as working and counter electrodes in a two-electrode system have been conducted in an alkaline solution. The electrochemical efficiency of cobalt ferrite toward overall electrochemical splitting of water was evaluated using linear sweep voltammetry (Figure 7a), and it was found that cobalt ferrite shows remarkable catalytic activity toward both anodic (OER) and cathodic (HER) processes. A 320 mV overpotential has been attained at the current density of 10 mA cm^{-2}. The favorable performance of these materials positions them as a charming alternate compared to expensive noble metal-based materials such as ruthenium-, iridium-, and platinum-based materials and their derivatives. The stability test for the overall electrochemical water splitting has also been studied via chronoamperometry with a two-electrode system. It was observed that the fabricated electrode exhibited the maintained stability after 10 h at an overpotential of 340 mV as shown in

https://doi.org/10.1021/acsomega.3c03314
ACS Omega 2023, 8, 37927–37935

Figure 7b. A comparative behavior of the currently reported electrocatalyst with previously reported materials is given in Table S1 in the Supporting Information.

4. CONCLUSIONS

We reported a flexible fibrous structure electrocatalyst in a three-electrode system and also studied its electrochemical performance in overall electrochemical water splitting. Cobalt ferrite ($CoFe_2O_4$) was deposited over carbon nanotube (CNT) fiber via a simple hydrothermal method. Surface morphology and elemental analysis were performed, and outcomes illustrated the clear picture of nanoparticle deposition and uniform dispersal on the CNTF surface. According to results of linear sweep voltammetry, the modified electrode displayed a lower overpotential value of 260 mV at 10 mA cm^{-2}, with a Tafel slope of 149 mV dec^{-1}. These findings indicate that cobalt ferrite serves as an effective catalyst in water electrolysis. Thorough examination of cyclic voltammetry (CV) showed that the modified fiber exhibited a notable increase in double capacitance, indicating its enhanced ability to store and release charges as compared to the pristine fiber. Additionally, electrochemical impedance revealed that the modified fiber displayed a significant reduction in charge transfer resistance, indicating efficient charge transfer kinetics. These improvements suggest an enhanced capacitive behavior and efficient charge transfer kinetics at the electrode interface. Moreover, the overall water splitting achieved an overpotential value of 320 mV at 10 mA cm^{-2} with reasonable stability. This dual functionality makes the cobalt ferrite-based composite fiber a promising candidate for efficient and sustainable electrochemical water splitting.

■ ASSOCIATED CONTENT

Supporting Information

The Supporting Information is available free of charge at https://pubs.acs.org/doi/10.1021/acsomega.3c03314.

SEM analysis after OER and comparative table for different electrocatalysts (PDF)

■ AUTHOR INFORMATION

Corresponding Authors

Munawar Iqbal − *Department of Chemistry, Division of Science and Technology, University of Education Lahore, Lahore 54770, Pakistan;* orcid.org/0000-0001-7393-8065; Email: munawar.iqbal@ue.edu.pk

Raqiqa Tur Rasool − *Department of Physics, Zhejiang Normal University, Jinhua, Zhejiang 321004, China;* Email: ra_chem@yahoo.com

Sheza Muqaddas − *Department of Chemistry, The University of Lahore, Lahore 54590, Pakistan;* Email: shezamuqaddas176@gmail.com

Abid Ali − *Department of Chemistry, The University of Lahore, Lahore 54590, Pakistan;* orcid.org/0000-0002-0452-4827; Phone: +92 321 5051352; Email: abid.ali@chem.uol.edu.pk, abidjaffer43@gmail.com

Authors

Aneesa Fatima − *Department of Chemistry, The University of Lahore, Lahore 54590, Pakistan*

Haia Aldosari − *Department of Physics, College of Science, Shaqra University, Shaqra 11961, Saudi Arabia*

M. S. Al-Buriahi − *Department of Physics, Sakarya University, Sakarya 54050, Turkey*

Maryam Al Huwayz − *Department of Chemistry, College of Science, Princess Nourah bint Abdulrahman University, Riyadh 11671, Saudi Arabia*

Z. A. Alrowaili − *Department of Physics, College of Science, Jouf University, Sakaka 42421, Saudi Arabia*

Mohammed S. Alqahtani − *Department of Radiological Sciences, College of Applied Medical Sciences, King Khalid University, Abha 61421, Saudi Arabia*

Muhammad Ajmal − *Department of Chemistry, Division of Science and Technology, University of Education Lahore, Lahore 54770, Pakistan*

Arif Nazir − *Department of Chemistry, The University of Lahore, Lahore 54590, Pakistan*

Complete contact information is available at: https://pubs.acs.org/10.1021/acsomega.3c03314

Author Contributions

A.A. and S.M. supervised the generated idea to use the CNTFs as electrode materials, A.F. did the electrochemical work and electrode fabrication, and H.A., M.S.A.-B., M.A.H., Z.A.A., and M.S.A. helped with characterizing the materials (SEM, EDX, and XRD), while M.A., A.N., M.I., and R.T.R. assist in the write-up and technical data handling of the manuscript.

Notes

The authors declare no competing financial interest.

■ ACKNOWLEDGMENTS

The authors are highly thankful to the Princess Nourah bint Abdulrahman University Researchers Supporting Project Number (PNURSP2023R439), Princess Nourah bint Abdulrahman University, Riyadh, Saudi Arabia. Furthermore, the authors also extend their gratitude to the Deanship of Scientific Research at King Khalid University, Saudi Arabia, for funding this work under the research group program number RGP2/515/44.

■ REFERENCES

(1) Schmidt, D. G. Research Opportunities for Future Energy Technologies. *ACS Energy Lett.* **2016**, *1* (1), 244−245.

(2) Daiyan, R.; MacGill, I.; Amal, R. Opportunities and Challenges for Renewable Power-to-X. *ACS Energy Lett.* **2020**, *5* (12), 3843−3847.

(3) Khan, M. A.; Zhao, H.; Zou, W.; Chen, Z.; Cao, W.; Fang, J.; Xu, J.; Zhang, L.; Zhang, J. Recent progresses in electrocatalysts for water electrolysis. *Electrochem. Energy Rev.* **2018**, *1*, 483−530.

(4) Zhang, X.; Zhao, H.; Li, C.; Li, S.; Liu, K.; Wang, L. Facile coordination driven synthesis of metal-organic gels toward efficiently electrocatalytic overall water splitting. *Appl. Catal., B* **2021**, *299*, No. 120641.

(5) Zhu, J.; Hu, L.; Zhao, P.; Lee, L. Y. S.; Wong, K.-Y. Recent advances in electrocatalytic hydrogen evolution using nanoparticles. *Chem. Rev.* **2020**, *120* (2), 851−918.

(6) Chen, X.; Li, C.; Grätzel, M.; Kostecki, R.; Mao, S. S. Nanomaterials for renewable energy production and storage. *Chem. Soc. Rev.* **2012**, *41* (23), 7909−7937.

(7) Anantharaj, S.; Ede, S. R.; Sakthikumar, K.; Karthick, K.; Mishra, S.; Kundu, S. Recent trends and perspectives in electrochemical water splitting with an emphasis on sulfide, selenide, and phosphide catalysts of Fe, Co, and Ni: a review. *ACS Catal.* **2016**, *6* (12), 8069−8097.

(8) Ren, H.; Yu, L.; Yang, L.; Huang, Z.-H.; Kang, F.; Lv, R. Efficient electrocatalytic overall water splitting and structural evolution of

cobalt iron selenide by one-step electrodeposition. *J. Energy Chem.* **2021**, *60*, 194−201.
(9) Ferreira, A. F.; Marques, A. C.; Batista, A. P.; Marques, P. A. S. S.; Gouveia, L.; Silva, C. M. Biological hydrogen production by Anabaena sp.−yield, energy and CO2 analysis including fermentative biomass recovery. *Int. J. Hydrogen Energy* **2012**, *37* (1), 179−190.
(10) Abdalla, A. M.; Hossain, S.; Nisfindy, O. B.; Azad, A. T.; Dawood, M.; Azad, A. K. Hydrogen production, storage, transportation and key challenges with applications: A review. *Energy Convers. Manage.* **2018**, *165*, 602−627.
(11) Zaik, K. Hydrogen-to-X application pathways overview. *CONTEMPORARY PROBLEMS OF POWER ENGINEERING AND ENVIRONMENTAL PROTECTION*. 2020, *207*.
(12) Ali, M.; Pervaiz, E.; Rabi, O. Enhancing the overall electrocatalytic water-splitting efficiency of Mo2C nanoparticles by forming hybrids with UiO-66 MOF. *ACS Omega* **2021**, *6* (50), 34219−34228.
(13) Arregi, A.; Amutio, M.; Lopez, G.; Bilbao, J.; Olazar, M. Evaluation of thermochemical routes for hydrogen production from biomass: A review. *Energy Convers. Manage.* **2018**, *165*, 696−719.
(14) Dincer, I. Green methods for hydrogen production. *Int. J. Hydrogen Energy* **2012**, *37* (2), 1954−1971.
(15) Shi, Y.; Zhang, B. Recent advances in transition metal phosphide nanomaterials: synthesis and applications in hydrogen evolution reaction. *Chem. Soc. Rev.* **2016**, *45* (6), 1529−1541.
(16) Xiao, P.; Chen, W.; Wang, X. A review of phosphide-based materials for electrocatalytic hydrogen evolution. *Adv. Energy Mater.* **2015**, *5* (24), 1500985.
(17) Shiva Kumar, S.; Himabindu, V. Hydrogen production by PEM water electrolysis−A review. *Mater. Sci. Energy Technol.* **2019**, *2* (3), 442−454.
(18) Kalamaras, C. M.; Efstathiou, A. M. In *Hydrogen production technologies: current state and future developments*; Conference papers in science, Hindawi: 2013.
(19) Cozzarini, L.; Bertolini, G.; Šuran-Brunelli, S. T.; Radivo, A.; Bracamonte, M. V.; Tavagnacco, C.; Goldoni, A. Metal decorated carbon nanotubes for electrocatalytic water splitting. *Int. J. Hydrogen Energy* **2017**, *42* (30), 18763−18773.
(20) Ursua, A.; Gandia, L. M.; Sanchis, P. Hydrogen production from water electrolysis: current status and future trends. *Proc. IEEE* **2012**, *100* (2), 410−426.
(21) Carmo, M.; Fritz, D. L.; Mergel, J.; Stolten, D. A comprehensive review on PEM water electrolysis. *Int. J. Hydrogen Energy* **2013**, *38* (12), 4901−4934.
(22) Yuan, Q.; Yu, Y.; Gong, Y.; Bi, X. Three-dimensional N-doped carbon nanotube frameworks on Ni foam derived from a metal−organic framework as a bifunctional electrocatalyst for overall water splitting. *ACS Appl. Mater. Interfaces* **2020**, *12* (3), 3592−3602.
(23) Acar, C.; Dincer, I. Review and evaluation of hydrogen production options for better environment. *J. Cleaner Prod.* **2019**, *218*, 835−849.
(24) Nikolaidis, P.; Poullikkas, A. A comparative overview of hydrogen production processes. *Renewable Sustainable Energy Rev.* **2017**, *67*, 597−611.
(25) Singh, S.; Jain, S.; PS, V.; Tiwari, A. K.; Nouni, M. R.; Pandey, J. K.; Goel, S. Hydrogen: A sustainable fuel for future of the transport sector. *Renewable Sustainable Energy Rev.* **2015**, *51*, 623−633.
(26) Fabbri, E.; Habereder, A.; Waltar, K.; Kötz, R.; Schmidt, T. J. Developments and perspectives of oxide-based catalysts for the oxygen evolution reaction. *Catal. Sci. Technol.* **2014**, *4* (11), 3800−3821.
(27) Casalongue, H. S.; Kaya, S.; Viswanathan, V.; Miller, D. J.; Friebel, D.; Hansen, H. A.; Nørskov, J. K.; Nilsson, A.; Ogasawara, H. Direct observation of the oxygenated species during oxygen reduction on a platinum fuel cell cathode. *Nat. Commun.* **2013**, *4* (1), 2817.
(28) Chen, G.; Ma, T. Y.; Liu, Z.; Li, N.; Su, Y.; Davey, K.; Qiao, S. Efficient and stable bifunctional electrocatalysts Ni/NixMy (M= P, S) for overall water splitting. *Adv. Funct. Mater.* **2016**, *26* (19), 3314−3323.
(29) Menezes, P. W.; Panda, C.; Loos, S.; Bunschei-Bruns, F.; Walter, C.; Schwarze, M.; Deng, X.; Dau, H.; Driess, M. A structurally versatile nickel phosphite acting as a robust bifunctional electrocatalyst for overall water splitting. *Energy Environ. Sci.* **2018**, *11* (5), 1287−1298.
(30) Suen, N.-T.; Hung, S.-F.; Quan, Q.; Zhang, N.; Xu, Y.-J.; Chen, H. M. Electrocatalysis for the oxygen evolution reaction: recent development and future perspectives. *Chem. Soc. Rev.* **2017**, *46* (2), 337−365.
(31) Wang, J.; Wei, Z.; Mao, S.; Li, H.; Wang, Y. Highly uniform Ru nanoparticles over N-doped carbon: pH and temperature-universal hydrogen release from water reduction. *Energy Environ. Sci.* **2018**, *11* (4), 800−806.
(32) Gao, M.; Tian, F.; Guo, Z.; Zhang, X.; Li, Z.; Zhou, J.; Zhou, X.; Yu, Y.; Yang, W. Mutual-modification effect in adjacent Pt nanoparticles and single atoms with sub-nanometer inter-site distances to boost photocatalytic hydrogen evolution. *Chem. Eng. J.* **2022**, *446*, No. 137127.
(33) Zhang, X.; Zhu, C.; Qiu, L.; Gao, M.; Tian, F.; Liu, Y.; Yang, W.; Yu, Y. Concentrating photoelectrons on sulfur sites of ZnxCd1−xS to active H−OH bond of absorbed water boosts photocatalytic hydrogen generation. *Surf. Interfaces* **2022**, *34*, No. 102312.
(34) Wang, Y.; Qiu, L.; Bao, S.; Tian, F.; Sheng, J.; Yang, W.; Yu, Y. Visible-light enhanced peroxymonosulfate activation on Co3O4/MnO2 for the degradation of tetracycline: Cooperation of radical and non-radical mechanisms. *Sep. Purif. Technol.* **2023**, *316*, No. 123779.
(35) Anantharaj, S.; Karthik, P. E.; Subramanian, B.; Kundu, S. Pt nanoparticle anchored molecular self-assemblies of DNA: an extremely stable and efficient HER electrocatalyst with ultralow Pt content. *ACS Catal.* **2016**, *6* (7), 4660−4672.
(36) Du, S.; Ren, Z.; Zhang, J.; Wu, J.; Xi, W.; Zhu, J.; Fu, H. Co 3 O 4 nanocrystal ink printed on carbon fiber paper as a large-area electrode for electrochemical water splitting. *Chem. Commun.* **2015**, *51* (38), 8066−8069.
(37) Anantharaj, S.; Jayachandran, M.; Kundu, S. Unprotected and interconnected Ru 0 nano-chain networks: advantages of unprotected surfaces in catalysis and electrocatalysis. *Chem. Sci.* **2016**, *7* (5), 3188−3205.
(38) Wang, M.; Wang, Z.; Gong, X.; Guo, Z. The intensification technologies to water electrolysis for hydrogen production−A review. *Renewable Sustainable Energy Rev.* **2014**, *29*, 573−588.
(39) Li, Y.; Huang, B.; Sun, Y.; Luo, M.; Yang, Y.; Qin, Y.; Wang, L.; Li, C.; Lv, F.; Zhang, W.; Guo, S. Multimetal borides nanochains as efficient electrocatalysts for overall water splitting. *Small* **2019**, *15* (1), 1804212.
(40) Geng, S.; Tian, F.; Li, M.; Liu, Y.; Sheng, J.; Yang, W.; Yu, Y.; Hou, Y. Activating interfacial S sites of MoS2 boosts hydrogen evolution electrocatalysis. *Nano Res.* **2022**, *15* (3), 1809−1816.
(41) Tahir, A.; Arshad, F.; Haq, T. u.; Hussain, I.; Hussain, S. Z.; Rehman, H. u. Roles of Metal Oxide Nanostructure-Based Substrates in Sustainable Electrochemical Water Splitting: Recent Development and Future Perspective. *ACS Appl. Nano Mater.* **2023**, *6* (3), 1631−1647.
(42) Ren, X.; Li, M.; Qiu, L.; Guo, X.; Tian, F.; Han, G.; Yang, W.; Yu, Y. Cationic vacancies and interface engineering on crystalline−amorphous gamma-phase Ni−Co oxyhydroxides achieve ultrahigh mass/areal/volumetric energy density flexible all-solid-state asymmetric supercapacitor. *J. Mater. Chem. A* **2023**, *11* (11), 5754−5765.
(43) Bhanja, P.; Kim, Y.; Paul, B.; Lin, J.; Alshehri, S. M.; Ahamad, T.; Kaneti, Y. V.; Bhaumik, A.; Yamauchi, Y. Facile Synthesis of Nanoporous Transition Metal-Based Phosphates for Oxygen Evolution Reaction. *ChemCatChem* **2020**, *12* (7), 2091−2096, DOI: 10.1002/cctc.201901803.
(44) Septiani, N. L. W.; Kaneti, Y. V.; Fathoni, K. B.; Kani, K.; Allah, A. E.; Yuliarto, B.; Nugraha; Dipojono, H. K.; Alothman, Z. A.; Golberg, D.; Yamauchi, Y. Self-Assembly of Two-Dimensional Bimetallic Nickel−Cobalt Phosphate Nanoplates into One-Dimensional Porous Chainlike Architecture for Efficient Oxygen Evolution

Reaction. *Chem. Mater.* **2020**, *32* (16), 7005−7018, DOI: 10.1021/acs.chemmater.0c02385.
(45) Guo, X.; Li, M.; Qiu, L.; Tian, F.; He, L.; Geng, S.; Liu, Y.; Song, Y.; Yang, W.; Yu, Y. Engineering electron redistribution of bimetallic phosphates with CeO2 enables high-performance overall water splitting. *Chem. Eng. J.* **2023**, *453*, No. 139796.
(46) Hu, S.; Wang, S.; Feng, C.; Wu, H.; Zhang, J.; Mei, H. Novel MOF-Derived Nickel Nitride as High-Performance Bifunctional Electrocatalysts for Hydrogen Evolution and Urea Oxidation. *ACS Sustainable Chem. Eng.* **2020**, *8* (19), 7414−7422.
(47) Ao, K.; Wei, Q.; Daoud, W. A. MOF-Derived Sulfide-Based electrocatalyst and Scaffold for Boosted Hydrogen Production. *ACS Appl. Mater. Interfaces* **2020**, *12* (30), 33595−33602.
(48) Guo, Y.; Zhang, C.; Zhang, J.; Dastafkan, K.; Wang, K.; Zhao, C.; Shi, Z. Metal−Organic Framework-Derived Bimetallic NiFe selenide Electrocatalysts with Multiple Phases for Efficient Oxygen Evolution Reaction. *ACS Sustainable Chem. Eng.* **2021**, *9* (5), 2047−2056.
(49) Han, G.; Li, M.; Liu, H.; Zhang, W.; He, L.; Tian, F.; Liu, Y.; Yu, Y.; Yang, W.; Guo, S. Short-Range Diffusion Enables General Synthesis of Medium-Entropy Alloy Aerogels. *Adv. Mater.* **2022**, *34* (30), 2202943 DOI: 10.1002/adma.202202943.
(50) Hutchings, G. S.; Zhang, Y.; Li, J.; Yonemoto, B. T.; Zhou, X.; Zhu, K.; Jiao, F. In situ formation of cobalt oxide nanocubanes as efficient oxygen evolution catalysts. *J. Am. Chem. Soc.* **2015**, *137* (12), 4223−4229.
(51) McEnaney, J. M.; Soucy, T. L.; Hodges, J. M.; Callejas, J. F.; Mondschein, J. S.; Schaak, R. E. Colloidally-synthesized cobalt molybdenum nanoparticles as active and stable electrocatalysts for the hydrogen evolution reaction under alkaline conditions. *J. Mater. Chem. A* **2016**, *4* (8), 3077−3081.
(52) Deng, X.; Tüysüz, H. Cobalt-oxide-based materials as water oxidation catalyst: recent progress and challenges. *ACS Catal.* **2014**, *4* (10), 3701−3714.
(53) Fominykh, K.; Feckl, J. M.; Sicklinger, J.; Döblinger, M.; Böcklein, S.; Ziegler, J.; Peter, L.; Rathousky, J.; Scheidt, E. W.; Bein, T.; Fattakhova-Rohlfing, D. Ultrasmall dispersible crystalline nickel oxide nanoparticles as high-performance catalysts for electrochemical water splitting. *Adv. Funct. Mater.* **2014**, *24* (21), 3123−3129.
(54) Gong, M.; Dai, H. A mini review of NiFe-based materials as highly active oxygen evolution reaction electrocatalysts. *Nano Res.* **2015**, *8*, 23−39.
(55) Sadiek, I. M.; Mohammad, A. M.; El-Shakre, M. E.; El-Deab, M. S. Electrocatalytic activity of nickel oxide nanoparticles-modified electrodes: Optimization of the loading level and operating pH towards the oxygen evolution reaction. *Int. J. Hydrogen Energy* **2012**, *37* (1), 68−77.
(56) Singh, A.; Chang, S. L.; Hocking, R. K.; Bach, U.; Spiccia, L. Highly active nickel oxide water oxidation catalysts deposited from molecular complexes. *Energy Environ. Sci.* **2013**, *6* (2), 579−586.
(57) Chen, M.; Wu, Y.; Han, Y.; Lin, X.; Sun, J.; Zhang, W.; Cao, R. An iron-based film for highly efficient electrocatalytic oxygen evolution from neutral aqueous solution. *ACS Appl. Mater. Interfaces* **2015**, *7* (39), 21852−21859.
(58) Trotochaud, L.; Young, S. L.; Ranney, J. K.; Boettcher, S. W. Nickel−iron oxyhydroxide oxygen-evolution electrocatalysts: the role of intentional and incidental iron incorporation. *J. Am. Chem. Soc.* **2014**, *136* (18), 6744−6753.
(59) Smith, R. D.; Prévot, M. S.; Fagan, R. D.; Zhang, Z.; Sedach, P. A.; Siu, M. K. J.; Trudel, S.; Berlinguette, C. P. Photochemical route for accessing amorphous metal oxide materials for water oxidation catalysis. *Science* **2013**, *340* (6128), 60−63.
(60) Zhu, H.; Zhang, S.; Huang, Y.-X.; Wu, L.; Sun, S. Monodisperse M x Fe3−x O4 (M= Fe, Cu, Co, Mn) nanoparticles and their electrocatalysis for oxygen reduction reaction. *Nano Lett.* **2013**, *13* (6), 2947−2951.
(61) Wei, C.; Feng, Z.; Baisariyev, M.; Yu, L.; Zeng, L.; Wu, T.; Zhao, H.; Huang, Y.; Bedzyk, M. J.; Sritharan, T.; Xu, Z. J. Valence change ability and geometrical occupation of substitution cations determine the pseudocapacitance of spinel ferrite XFe2O4 (X= Mn, Co, Ni, Fe). *Chem. Mater.* **2016**, *28* (12), 4129−4133.
(62) Chen, J.; Zhao, D.; Diao, Z.; Wang, M.; Guo, L.; Shen, S. Bifunctional modification of graphitic carbon nitride with MgFe2O4 for enhanced photocatalytic hydrogen generation. *ACS Appl. Mater. Interfaces* **2015**, *7* (33), 18843−18848.
(63) Lu, X.-F.; Gu, L.-F.; Wang, J.-W.; Wu, J.-X.; Liao, P.-Q.; Li, G.-R. Bimetal-Organic Framework Derived CoFe2O4/C Porous Hybrid Nanorod Arrays as High-Performance Electrocatalysts for Oxygen Evolution Reaction. *Adv. Mater.* **2017**, *29* (3), 1604437 DOI: 10.1002/adma.201604437.
(64) Yan, K.-L.; Shang, X.; Liu, Z.-Z.; Dong, B.; Lu, S.-S.; Chi, J.-Q.; Gao, W.-K.; Chai, Y.-M.; Liu, C.-G. A facile method for reduced CoFe2O4 nanosheets with rich oxygen vacancies for efficient oxygen evolution reaction. *Int. J. Hydrogen Energy* **2017**, *42* (38), 24150−24158.
(65) Ding, Y.; Zhao, J.; Zhang, W.; Zhang, J.; Chen, X.; Yang, F.; Zhang, X. Single-walled carbon nanotubes wrapped CoFe2O4 nanorods with enriched oxygen vacancies for efficient overall water splitting. *ACS Appl. Energy Mater.* **2019**, *2* (2), 1026−1032.
(66) Ji, X.; Hao, S.; Qu, F.; Liu, J.; Du, G.; Asiri, A. M.; Chen, L.; Sun, X. Core−shell CoFe 2 O 4@ Co−Fe−Bi nanoarray: a surface-amorphization water oxidation catalyst operating at near-neutral pH. *Nanoscale* **2017**, *9* (23), 7714−7718.
(67) Rana, S.; Yadav, K. K.; Guchhait, S. K.; Nishanthi, S. T.; Mehta, S. K.; Jha, M. Insights of enhanced oxygen evolution reaction of nanostructured cobalt ferrite surface. *J. Mater. Sci.* **2021**, *56*, 8383−8395.
(68) Zhang, Z.; Zhang, J.; Wang, T.; Li, Z.; Yang, G.; Bian, H.; Li, J.; Gao, D. Durable oxygen evolution reaction of one dimensional spinel CoFe 2 O 4 nanofibers fabricated by electrospinning. *RSC Adv.* **2018**, *8* (10), 5338−5343.